Atmospheric Environment 81 (2013) 136–147

Contents lists available at ScienceDirect

Atmospheric Environment

journal homepage: www.elsevier.com/locate/atmosenv

Remote sensing of surface visibility from space: A look at the United States East Coast

Amy L. Kessner [a], Jun Wang [a, *], Robert C. Levy [b], Peter R. Colarco [c]

[a] University of Nebraska – Lincoln, Lincoln, NE, USA
[b] Climate and Radiation Lab, Code 613, NASA Goddard Space Flight Center, Greenbelt, MD, USA
[c] Atmospheric Chemistry and Dynamics Lab, Code 614, NASA Goddard Space Flight Center, Greenbelt, MD, USA

HIGHLIGHTS

- First application of satellite (MODIS) data to estimate cloud-free surface visibility over land.
- A quality control procedure is developed for the one-min surface extinction coefficient data from the visibility sensors.
- Multi-year analysis shows the promise of estimating surface visibility from space in summer over U.S. East Coast.
- Treatment of aerosols above boundary layer is important for derivation of surface visibility from aerosol optical depth.

ARTICLE INFO

Article history:
Received 25 March 2013
Received in revised form
23 August 2013
Accepted 27 August 2013

Keywords:
Visibility
Remote sensing
Aerosol optical depth
MODIS
GEOS-5

ABSTRACT

Measurement of surface visibility is important for the management of air quality, human health, and transportation. Currently, visibility measurements are only available through ground-based instrumentation, such as the Automated Surface Observing System (ASOS), and therefore lack spatial coverage. In analogy to the recent work of using satellite-based aerosol optical depth (AOD) to derive surface dry aerosol mass concentration at continental-to-global scale for cloud-free conditions, this study evaluates the potential of AOD retrieved from the MODerate Resolution Imaging Spectroradiometer (MODIS) for deriving surface visibility. For this purpose of evaluation the truncated (up to ~16 km or 10 miles) and discrete (at the interval no less than 0.4 km or 1/4 mile) visibility data from hourly operational weather reports are not suitable, and the ASOS-measured one-minute raw surface extinction coefficient (b_{ext}) values have to be used. Consequently, a method for quality control on the b_{ext} data is first developed to eliminate frequent problems such as extraneous points, poor calibration, and bad formatting, after which reliable b_{ext} data are obtained to estimate the surface visibility. Subsequent analysis of the AOD and b_{ext} relationship on the East Coast of the United States reveals their average linear correlation coefficient (R) of 0.61 for all twelve (2000–2011) years of data at 32 ASOS stations, with the highest R value in summer and the lowest values in fall and winter. Incorporation of the Goddard Earth Observing System, Version 5 (GEOS-5) modeled vertical profile of aerosols into the derivation of visibility from AOD is evaluated for two methods, one scaling the modeled surface b_{ext} with the ratio of MODIS AOD to the modeled AOD, and another scaling the ratio of modeled AOD in the boundary layer to total columnar AOD with the MODIS AOD and assuming well-mixed aerosol extinction in the boundary layer. Analysis with three summers (2003–2004, 2006) of available GEOS-5 data and ASOS data reveals that the second method is superior, and generates a regression model that, after independent evaluation for summer 2005, is found to be statistically robust with R of 0.70 and a mean bias of 0.32 km in derived visibility. This study is among the first to demonstrate the potential of using satellite-based aerosol product over land to operationally derive surface visibility.

1. Introduction

Visibility is the greatest horizontal distance at which it is just possible to observe and identify particular objects. Therefore, accurate measurement and forecast of atmospheric visibility is important for the safety of both aviation and ground transportation,

* Corresponding author. Tel.: +1 402 472 3597.
E-mail addresses: Agehring3@huskers.unl.edu (A.L. Kessner), Jwang7@unl.edu (J. Wang), Robert.c.levy@nasa.gov (R.C. Levy), Peter.r.colarco@nasa.gov (P.R. Colarco).

1352-2310/$ – see front matter © 2013 Elsevier Ltd. All rights reserved.
http://dx.doi.org/10.1016/j.atmosenv.2013.08.050

as well as for aesthetic reasons. Visibility can be reduced by natural conditions, such as clouds and fog, and also by the presence of aerosols, which can be natural or anthropogenic. Since heavy concentrations of aerosol (also known as particulate matter, PM) at Earth's surface are a component of poor air quality, accurate measurement and forecast of horizontal visibility can be useful for health applications.

A majority of poor visibility cases are often found to be a result of anthropogenic aerosols (Watson and Chow, 1994; Wang et al., 2009; Qu et al., 2013). Currently, the main legislation enforcing visibility standards in U.S. is the 1977 Clean Air Act, which mandates enforcement of visibility standards in national parks. However, visibility monitoring and protection is important in more urban areas as well. A 10% reduction in visibility was found to reduce nonfatal accidents by 15.6 units a day (Mensah and Osei-Adjei, 1991). There are monetary benefits as well. A study by Trijonis et al. (1985) found that a 10% improvement in visibility would produce financial benefits on order of hundreds of millions of dollars a year in regions such as Los Angeles and San Francisco. Furthermore, the U.S. Environmental Protection Agency report shows that the improvement in visibility (alone) due to the continuous implementation of the 1990 Clean Air Act Amendments can lead to residential and recreational benefits of more than $60 billion dollars by 2020 (USEPA, 2011). In order to best define when and where visibility is going to be a problem and how to improve it, accurate, global measurements are required. This study is among the first to conduct feasibility evaluations toward developing algorithms for global measurement for visibility from space.

Prior to 1990, most measurements of surface visibility were made by a human observer and thus were largely subjective. However, by the early 1990's, the Automated Surface Observing System (ASOS) began to replace human observation in the United States at many airports (NOAA et al., 1998). Yet, with coverage restricted to U.S. airports, the ASOS measurements cannot produce a complete picture of surface visibility. Satellite observations, on the other hand, are global, and can be used to retrieve aerosol properties. Additionally, with the implementation of automated visibility measurements from ASOS, the definition of visibility has been altered from a horizontal surface measurement to essentially a point measurement since ASOS does not consider the horizontal variation of aerosol beyond the path length of air ($\sim$1.0 m) that ASOS samples. This change is favorable for using satellite data to derive surface visibility because satellite data (such as AOD) often are columnar quantities at high spatial resolution, and similar to ASOS visibility, they are meant to be representative over a finite area (such as over 10 $\times$ 10 km^2, even though the ASOS-reported visibility can be larger than 10 km).

There have been many studies that characterize the relationship between AOD and surface PM (Hoff and Christopher, 2009). A global study by Van Donkelaar et al. (2006) showed correlations between 0.58 and 0.69 for daily AOD compared to $PM_{2.5}$ (PM having diameter $\leq$ 2.5 μm) averaged between 10:00 a.m. and 12:00 p.m. LT for the United States. These correlations were improved globally to between 0.77 and 0.83 when a chemical transport model (CTM) was incorporated to account for the vertical distribution of aerosol (Van Donkelaar et al., 2010). Other studies have shown significant correlation ($R > 0.6$) over portions of the United States, but also that the correlation varies by season (Wang and Christopher, 2003; Zhang et al., 2009; Green et al., 2009). This is because that many factors complicate the AOD-PM relationship such as aerosol size, aerosol type, relative humidity, and the vertical structure of aerosol extinction (Wang and Christopher, 2003; Van Donkelaar et al., 2006, 2010; Gupta et al., 2006). For example, the measurements of PM mass (for air quality applications) are usually taken in dry conditions (at temperature $\sim$50 °C, Watson et al., 1998; Allen et al., 1997), and hence do not take into account the ambient conditions of the atmosphere. However, relative humidity (RH) can affect the size and water content of an aerosol, and thus the scattering and absorbing properties (Tang and Munkelwitz, 1994; Wang et al., 2008). These factors can be partially overcome in the study of AOD-visibility relationship because AOD and visibility are both ambient optical quantities, affected by the same RH effect on particle extinction.

Few studies, however, have attempted to use satellite-retrieved AOD to infer visibility. An early study by Kaufman and Fraser (1983) showed a strong correlation of 0.85 between AOD and inverse visibility at Dulles airport during 1980 while a weaker correlation of 0.51 was found during 1981. Vermote et al. (2002) established a relation between AOD and visibility to be used for Visible/Infrared Imager/Radiometer Suite (VIIRS) data onboard the National Polar-orbiting Operational Environmental Satellite System (NPOESS). This relation developed for VIIRS was then used by Retalis et al. (2010) to determine AOD from visibility data in Cyprus. Fei et al. (2006) used principal component regression to retrieve visibility data over water in coastal China from NOAA/AVHRR satellite data within two emitted-infrared bands. A more recent study by Hadjimitsis et al. (2010) used the darkest pixel atmospheric correction algorithm on Landsat-5 TM data in cooperation with radiative transfer calculations to produce a horizontal visibility product.

To date, no past studies like this study, to our knowledge, used remotely sensed AOD in conjunction with modeled aerosol vertical profile to infer surface visibility for multiple years. To validate our results, we first develop a method of quality control for ASOS one-minute visibility data. Next, we conduct remote sensing of surface visibility on the East Coast of the United States in four parts: I) a long-term study of AOD versus visibility data, II) incorporation of the vertical profile of aerosol from an Earth system model using two methods for multiple years of data and compare the two methods with a baseline method that doesn't consider aerosol vertical profile, III) development and independent evaluation of the regression models established in part II using one year of data (not used in part II), and IV) a case demonstration of our best method (found in III) to an East Coast high-AOD event.

2. Relating AOD, visibility, and surface PM

AOD, PM, and visibility are physically related. AOD is defined as the integral of the aerosol extinction due to scattering and absorption:

$$\mathrm{AOD} = \int_0^z b_{\mathrm{ext}}(\mathrm{rh}(z))\mathrm{d}z \tag{1}$$

where b_{ext} is the atmospheric aerosol extinction coefficient, rh is the relative humidity, and z is the altitude.

To relate PM to AOD many complicating factors are involved:

$$\mathrm{AOD} = H \cdot \frac{3}{4} \cdot \mathrm{PM}\left(z_{\mathrm{sfc}}\right) \cdot \frac{f\left(\mathrm{rh}\left(z_{\mathrm{sfc}}\right)\right)}{\rho} \cdot \frac{Q_{\mathrm{dry}}}{r_{\mathrm{eff}}} \tag{2}$$

where $f(\mathrm{rh}(z_{\mathrm{sfc}}))$ is the relative humidity factor, z_{sfc} is the surface height, Q_{dry} is the extinction efficiency under dry conditions, r_{eff} is the effective radius, ρ is the aerosol mass density, and $H = \int_0^z b_{\mathrm{ext}}(\mathrm{rh}(z))/b_{\mathrm{ext}}(\mathrm{rh}(z_{sfc}))\mathrm{d}z$, the shape of aerosol extinction profile (Wang and Christopher, 2003; Koelemeijer et al., 2006).

Visibility is technically defined as the length of path in the atmosphere required to reduce the luminous flux in a collimated beam from an incandescent lamp, at a color temperature of 2700 K, to 5 percent of its original value (WMO, 2008). The Koschmieder equation defines visibility mathematically,

$$C = \exp\left(-\text{visibility}\cdot b_{\text{ext}}\left(\text{rh}\left(z_{\text{sfc}}\right)\right)\right) \quad (3)$$

and, when the visual contrast (C) is set to 5% (0.05), Visibility can be defined as (WMO, 2008; NCDC, 2003):

$$\text{Visibility} = \frac{3.0}{b_{\text{ext}}\left(\text{rh}\left(z_{\text{sfc}}\right)\right)}. \quad (4)$$

Thus, the relationship between visibility and AOD can be defined as:

$$\text{AOD} = \frac{3.0}{\text{visibility}}\cdot H. \quad (5)$$

Comparing Eq. (5) with Eq. (2), the simplicity of the AOD-visibility relationship when compared with the AOD-PM relationship can be seen. Additionally, the shape of the aerosol extinction profile (H) is an important link between AOD and the surface parameters PM and visibility.

3. Data

3.1. MODerate Resolution Imaging Spectroradiometer (MODIS)

This study uses the MODIS level 2 AOD product collection 5.1 from both Terra (morning observations; years 2000–2011) and Aqua (afternoon observations; years 2002–2011). MODIS measured radiances in the wide spectral range (0.47–2.13 μm) are used to retrieve AOD over land with better accuracy than previous satellite sensors (Levy et al., 2007). AOD data are 10 km in nominal spatial resolution, and in the latitudes studied here there is approximately one retrieval (if cloud free) per day, per satellite. During the retrieval process, quality assurance (QA) confidence flags with value between 0 (bad) and 3 (good) are assigned to the AOD retrieval (Remer et al., 2009). In this study, only AOD values with QA flag values of 2 or 3 are used.

3.2. The Goddard Earth Observing Systems model, Version 5 (GEOS-5)

The GEOS-5 model includes an atmospheric general circulation model, a module for treatment of atmospheric aerosols, and a data assimilation system (Rienecker et al., 2008). This study uses results of the GEOS-5 model driven with meteorological analyses provided by the Modern-Era Retrospective Analysis for Research and Applications (MERRA, Rienecker et al., 2011) and incorporating an aerosol module based on the Goddard Chemistry, Aerosol, Radiation, and Transport (GOCART) model (Colarco et al., 2010), which simulates the distributions of dust, sulfate, carbonaceous, and sea salt aerosols. The model was run at a horizontal spatial resolution of 0.625° longitude × 0.5° latitude (approximately 50 km-sized grid cells) with 72 vertical levels for the period 2003–2006.

Results incorporate assimilation of aerosol optical depth derived from MODIS observations. Using AERONET AOD observations as a standard, a neural network is employed to predict the MODIS AOD directly from the cloud-cleared MODIS reflectances. The assimilation takes full consideration of observation and background biases and errors (Dee and Da Silva, 1998, 1999), as well as quality control check (Dee et al., 2001). Similar to other past studies (Wang et al., 2004; Xu et al., 2013), the assimilation impacts the overall loading of aerosols in the model, but not their partition between simulated species or vertical profile.

3.3. The Automated Surface Observing System (ASOS)

Human observation of visibility is being replaced by the ASOS at ~1000 airports across the United States (NOAA et al., 1998). As many as three Belfort Model 6220 Visibility Sensor may be installed at any given ASOS station in order to provide more thorough coverage of an area (e.g. multiple runways) as well as provide back-up sensors in case the primary sensor fails. The transmitter in the visibility sensor contains a xenon flashtube that produces light in the ~300 nm–1100 nm wavelengths (EG&G Electro-Optics, 1983). The receiver is located at ~45° angle from the transmitter and is used to measure the forward scattered xenon light after passing through an optical longpass filter that attenuates any wavelengths below 515 nm. Through intercomparison testing, the model 6220 was found to have the same response to aerosols as it would if the emitter and receiver all operated at a single wavelength of 690 nm (C. Greenblatt, Belfort Instrument, 2012, personal communication). The sensor was initially calibrated by operating it near an Optec Transmissometer that measures the attenuation of light (both scattering and absorption) at 550 nm, defining the standard value for the extinction coefficient in relation to visibility (Molenar et al., 1992; NOAA et al., 1998). Thus, this calibration procedure leads to (and supports) the assumption:

$$b_{\text{sca}} = b_{\text{ext}}(550\ \text{nm}) \quad (6)$$

where b_{sca} is the ASOS-measured forward scattering coefficient and b_{ext} is the volume extinction coefficient at 550 nm. Errors may be introduced by this assumption by absorption in the atmosphere, but can be minimal over the U.S. East Coast where the average single scattering albedo is approximately 0.95 (Takemura et al., 2002). Therefore, this study will refer to the output from the ASOS visibility sensor's measurement of forward scattering as the extinction coefficient measured at 550 nm (b_{ext}).

The ASOS network consists of the National Weather Service (NWS) and Federal Aviation Association (FAA) sites. Visibility observations are made at a one-minute time resolution, but the standard product is reported hourly and at discrete values of M1/4SM (less than ¼ statute mile), 1/4SM, 1/2SM, 3/4SM, 1SM, 1 1/4SM, 1 1/2SM, 1 3/4SM, 2SM, 2 1/2SM, 3SM, 4SM, 5SM, 6SM, 7SM, 8SM, 9SM and 10SM (1 SM = 1.60934 km); any observation of visibility greater than 10SM (~16 km) is truncated into the reportable value of 10SM. Typical values of visibility under light, moderate, and heavy aerosol conditions are greater than 40 km (>25 SM), 15–40 km (9–25 SM), and less than 15 km (<9 SM), respectively. The coarse increments used for the hourly data are therefore unsuitable for our study as information under light and moderate aerosol conditions are binned up into a single bin (10 SM). Because of this limitation we employ the one-minute ASOS data, which are found online in the form of the National Climatic Data Center's Data Set 6405 and 6406 (NCDC's DSI-6405 and DSI-6406). These datasets contain raw meteorological measurements, including visibility (in the form of b_{ext} [km^{-1}]), taken at one-minute intervals, and thus are appropriate for the applications in this study. This study uses the one-minute ASOS data for the years 2000–2011. However, it is important to note that there are currently no quality controls in place for the one-minute ASOS data.

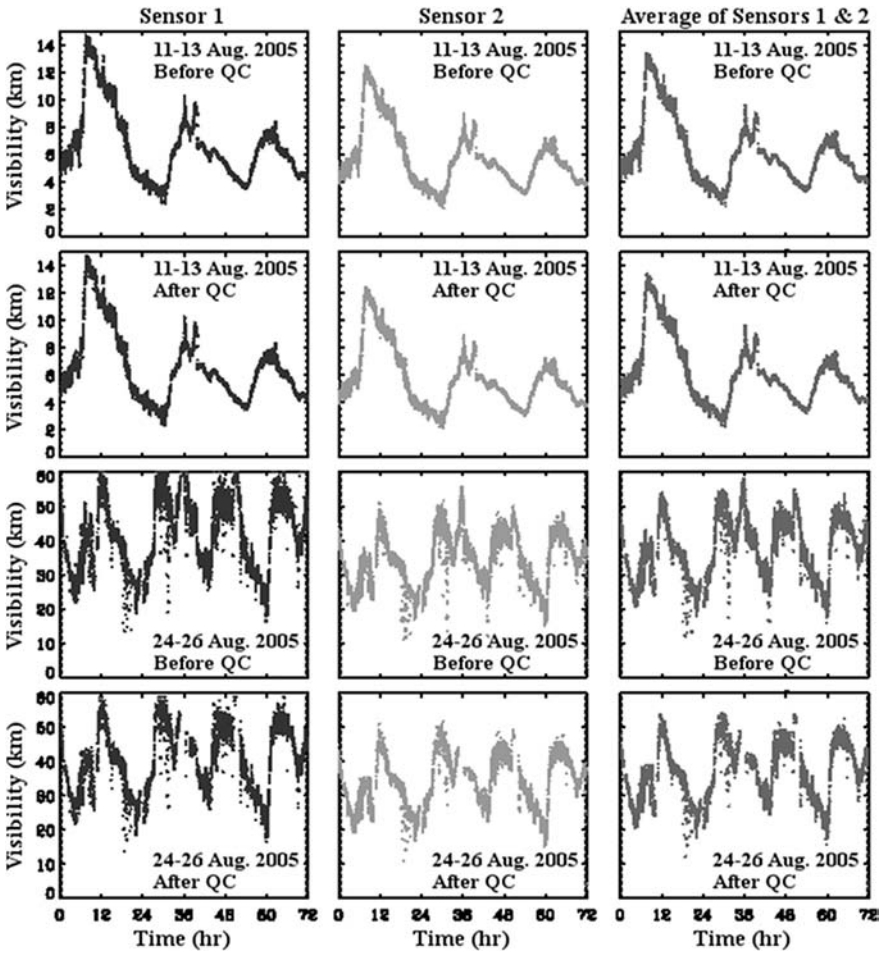

Fig. 1. Time series of ASOS visibility data at Baltimore/Washington International Thurgood Marshall Airport (KBWI) before and after quality control for (top 2 rows) 11–13 August 2005 and (bottom 2 rows) 24–26 August 2005. Time series is shown for (left column) the first visibility sensor (middle column), the second visibility sensor, and (right column) the average of both sensors. Time shown is in Local Time (EST).

4. ASOS one-minute data quality control method and results

4.1. Method

The stored ASOS one-minute extinction coefficient data do not undergo any quality control like the ASOS hourly data. Hence, before they are used to evaluate the visibility derived from MODIS AOD, we developed a quality control method to cope with such common problems in this dataset as unrealistic variability, poor calibration, and inconsistent formatting. The method is based upon work done by Richards et al. (1996), the Interagency Monitoring of Protected Visual Environments (IMPROVE) nephelometer (an instrument that measures ambient light scattering, b_{scat}) protocol (Cismoski, 1994), and the expected uncertainty (up to ±10%) of the Belfort Model 6220 Visibility Sensor (Crosby, 2003).

Since any ASOS station may contain up to three visibility sensors, the quality control implemented here needs to apply to stations either single sensors or multiple sensors (two or three). To ensure reliable and repeatable ASOS visibility data, we applied the following criteria to filter the ASOS one-minute b_{ext} data. A particular ASOS b_{ext} observation was retained if:

1) 0.05 km^{-1} < b_{ext} ≤ 7.5 km^{-1}. The IMPROVE protocol flags b_{scat} data when they exceed 5.0 km^{-1}. To include more low visibility measurements, a cut-off value of 7.5 km^{-1} (1/4 mile visibility) was selected for this study. Also, the ASOS one-minute data are truncated at 0.05 km^{-1} (the detection limit), so data of this value are excluded from this study.
2) *Relative Humidity* ≤ 95%. Relative humidity data are obtained from ASOS one-minute measurements. This quality control is an IMPROVE qualification, and was chosen for this study to eliminate data where fog or precipitation may be occurring.
3) The difference between one b_{ext} measurement and a three-minute running average of b_{ext} measurements should be ≤20%. The three-minute running average is computed by taking the average of ±1 min of data for each data point. This quality control was implemented to eliminate unrealistic variability and extraneous points within the data.

Additionally, for multi-sensor sites we require:

4) The difference between a three-minute rolling average of any two visibility sensors should be ≤20%. This quality control was implemented to eliminate poor calibration between sensors, as well as unrealistic variability that may exist in one sensor, but not the other(s). The value of 20% was chosen (a) because the Belfort visibility sensor has an accuracy of ±10% (Crosby, 2003), and (b) to obtain the data with highest quality as possible for the evaluation of our estimate of visibility from MODIS AOD.

4.2. Results of ASOS quality control

To demonstrate our quality control method, we select time series of visibility data for the Thurgood Marshall Baltimore/Washington International Airport (KBWI) during 11–13 August and 24–26 August 2005 (Fig. 1). These two time periods are selected not only to show the contrast between a period of poor visibility and a period of good visibility, but to demonstrate the effectiveness of multiple visibility sensors as well.

Low visibilities occurred during 11–13 August 2005 (Fig. 1). A diurnal cycle in visibility can be seen with the peak during the early afternoon each day and then decreasing into the night hours. Most of the data (95%) are retained during quality control. This shows that the ASOS visibility sensors at KBWI are in good agreement during this period, and thus the data quality is very high.

However, during 24–26 August 2005, a discernible difference can be seen between the ASOS visibility data before and after quality control as only 69% of the data are retained during this period (Fig. 1). This can be attributed to several factors: 1) the first visibility sensor reaching the truncation point (60 km or 0.05 km^{-1}), 2) a calibration difference between the first and second sensor, and 3) extraneous data points found in both sensors. Calibration differences between visibility sensors at a given ASOS station are, unfortunately, common. For this reason, during our long-term analysis only ASOS stations with two or three visibility sensors will be used.

To illustrate the effectiveness of our data quality control, we plot the histograms of KBWI visibility data for the year 2005 before and after quality control (Fig. 2). Before quality control, a noticeable difference in the shape of the histograms for each visibility sensor can be seen. Sensor 1 has a high relative frequency of visibilities in the 60 km bin while sensor 2 has a low relative frequency of visibilities in the same bin. This implies that sensor 1 is calibrated to output higher visibilities than sensor 2, which agrees with the time series shown in Fig. 1. After the data have undergone quality control, data with calibration differences greater than 20% have been removed. This results in the histograms becoming more consistent between the two sensors. During this process 34.0% of the ASOS visibility data are lost.

To further explore data loss due to our quality control, Table 1 lists the 32 ASOS stations within our study region and how much data is lost for each station for each quality control criteria for the year 2005. The station with the greatest data loss during this period is the Norfolk International Airport (KORF) with a loss of 99.9% of the data. This loss is contributed almost entirely to a calibration difference between the two sensors at this station. The station that retained the most data is the Ronald Reagan Washington National Airport (KDCA) with a loss of 32.7% of the data. For all stations a majority of data was lost during the 4th quality control criteria with an average of 52.2% data loss for two-sensor stations and 73.7% data loss for three-sensor stations (Table 1). The fewest data were lost during the 3rd quality control criteria with an average of 1.2% data loss for all stations. Again, it is important to reiterate that our purpose here is to keep the data that are assured with our best information to be in the highest quality. This assurance can come with a steep cost of data loss but is necessary for the most accurate results in the following sections.

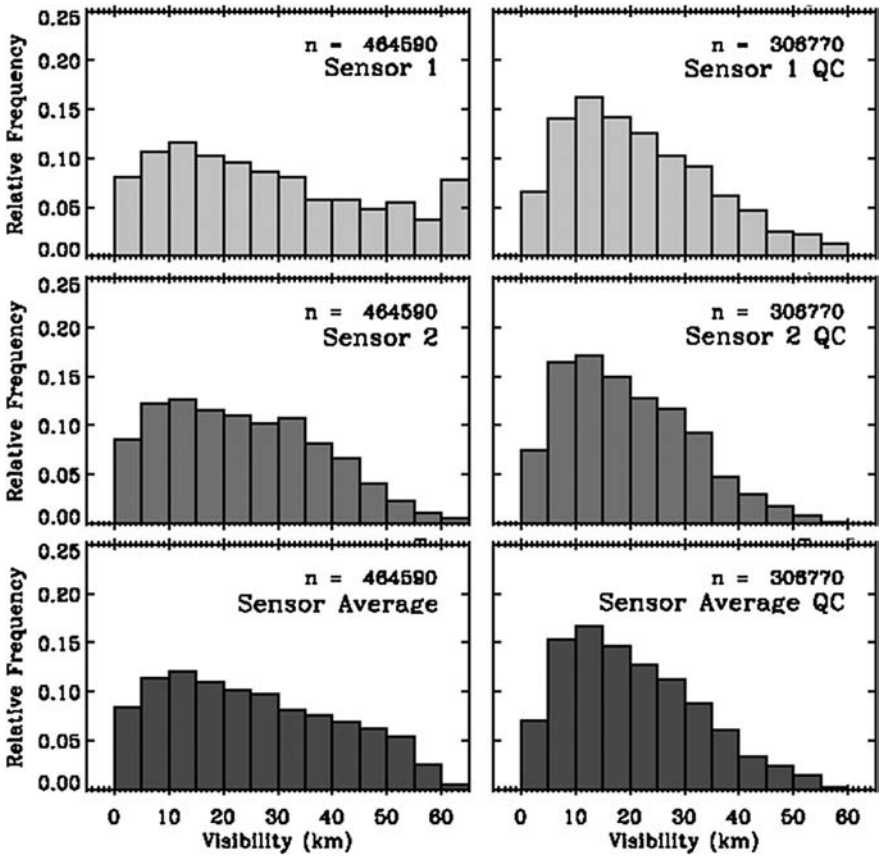

Fig. 2. Relative frequency histograms of ASOS visibility data at KBWI for 2005. Data are shown (left) before quality control and (right) after quality control as well as for (top row) the first visibility sensor (middle row), the second visibility sensor, and (bottom row) the average of both sensors.

Table 1
Percentage of data lost to each step of quality control for individual ASOS stations with multiple visibility sensors for the year 2005. Stations with three visibility sensors are marked with an asterisk*. Letters in first column correspond to the Taylor Diagrams in Fig. 5.

Station		QC 1 (%)	QC 2 (%)	QC 3 (%)	QC 4 (%)	Total (%)
A	KATL	0.9	9.6	1.3	66.7	70.1
B	KBDR	10.5	8.1	0.4	60.4	67.3
C	KBKW	9.4	13.2	1.1	95.8	97.0
D	KBNA	10.9	2.5	0.7	27.4	37.0
F	KBWI	8.2	6.4	0.3	24.5	34.0
G	KCLT	7.0	9.9	0.5	25.1	34.3
	KCMH	7.7	6.9	0.5	58.6	60.8
H	KCVG	8.9	6.9	0.6	57.4	61.5
I	KDCA	11.0	16.7	0.4	10.3	32.7
	KDTW	27.7	11.9	0.5	85.2	88.9
	KERI	18.0	58.7	9.4	72.8	89.0
J	KEWR	3.0	6.5	0.9	26.9	32.8
K	KGRR	15.7	10.7	0.8	65.5	69.3
L	KISP	27.3	37.7	0.7	45.8	74.8
	KMDW	24.3	10.9	1.0	85.2	86.1
N	KMEM	6.2	1.6	0.4	43.1	45.1
O	KMKE	20.6	5.9	0.6	62.5	74.8
P	KMKG	10.1	11.4	2.4	56.2	64.0
	KORD	20.8	11.3	0.9	57.3	69.1
	KORF	15.5	16.2	0.5	99.4	99.9
Q	KPIT	29.3	30.2	1.4	57.6	71.6
R	KPVD	18.3	11.5	0.4	23.9	43.1
S	KPWM	8.0	61.5	0.6	23.7	70.4
T	KRDU	1.5	12.6	1.4	26.2	34.0
U	KSYR	32.2	6.2	1.1	47.1	70.7
	KBDL*	27.3	15.3	15.3	58.0	76.7
E	KBOS*	27.1	8.3	1.1	62.1	76.5
	KCLE*	1.5	1.4	0.8	70.9	71.6
L	KIAD*	15.1	5.9	1.7	88.1	92.2
	KJFK*	7.6	5.1	0.8	95.7	96.3
M	KLGA*	21.0	5.8	0.5	75.4	78.6
	KPHL*	12.6	6.2	3.2	66.0	70.9
All station average:		14.5	13.5	1.2	56.9	66.9
2 sensor average:		14.1	15.4	1.1	52.2	63.1
3 sensor average:		16.0	6.9	1.4	73.7	80.4

5. Derivation of visibility from MODIS AOD

5.1. Long-term analysis of AOD vs. visibility

The establishment of a quality control regime for the ASOS one-minute b_{ext} data allows these data to be used in the analysis of the relationship between surface visibility (or b_{ext}) and MODIS AOD. To collocate MODIS and ASOS, the MODIS AOD pixel that is centered over the ASOS station is first determined based upon the distances; then, this MODIS AOD pixel and the surrounding 24 pixels (within a 5 × 5 pixel box) are retained (e.g. Ichoku et al., 2002). A spatial average of MODIS AOD over these pixels (e.g. 50 km × 50 km area) is used for comparison with ±30 min temporal averages of b_{ext} from the MODIS overpass time (e.g. Ichoku et al., 2002). Furthermore, at least 5 valid out of a possible 25 pixels are required for spatial averaging to help reduce the AOD errors due to cloud contamination (e.g. Levy et al., 2003). In the temporal average, at least 50% of the data must be retained after ASOS quality control is performed. Furthermore, the average of the visibility from all sensors at any given ASOS station is used.

ASOS stations used in the long-term (2000–2011) analysis of AOD and visibility are shown in Fig. 3A, including 25 two-sensor stations and 7 three-sensor stations. Correlation coefficients of ASOS hourly-averaged b_{ext} data vs. a MODIS AOD 5 × 5 pixel average for the 32 stations are shown in Fig. 3B for all years of data. Circles outlined in red are insignificant according to the two-tailed t-statistic test ($p > 0.01$) or have three or fewer available collocated points. The maximum correlation is 0.93 at the Chicago Midway International Airport (KMDW) and the minimum significant correlation is 0.24 at the Rayleigh County Memorial Airport (KBKW). The reason for this large difference in correlation is uncertain. There are many possibilities for the high correlation at KMDW including a small number of collocated points ($N = 7$) as well as all of the AOD retrievals having a value greater than 0.2. The low correlation at KBKW may be due to a poor correlation during the spring and fall ($R = 0.19$ and $R = 0.08$, respectively). The mean of all statistically significant correlation coefficients is 0.61 and the median correlation value is 0.63 for all 12 years of data.

Seasonally, geographical distributions of correlation coefficients are also shown for spring (MAM, Fig. 3C), summer (JJA, Fig. 3D), fall (SON, Fig. 3E), and winter (DJF, Fig. 3F) for all 12 years of data. Summer shows the highest correlations with a mean and median of 0.69 for statistically significant data. Following summer is fall with a mean and median of 0.56. Spring has a mean of 0.55 and a median of 0.59 while winter has the lowest correlations with a mean of 0.53 and a median of 0.45.

To further explore the seasonal relationship between AOD and b_{ext}, monthly correlations are explored for the years 2000–2011 (Fig. 4). Once again, the highest correlations are found in the summer months with the highest value $R = 0.70$ in July. The lowest correlations are in the fall and winter months with the lowest correlation, $R = 0.30$, in November. Interestingly, there is a strong correlation ($R = 0.75$) between the monthly R-values and the number of collocated points for that month. This behavior of monthly R-values and correlations with number of points has many possible reasons:

1) There are high correlations in the summer because both AOD and surface visibility have a larger signal range. While the absolute uncertainties for each dataset may be large, their relative uncertainties are smaller. Both the MODIS and ASOS sensors retrieve more accurately when there is significant amount of aerosol/extinction in the atmosphere, which happens most often during the summer.
2) There are low correlations in winter because the relative uncertainties of both measurements are large.
3) In the winter months the planetary boundary layer (PBL) is often stable, suppressing aerosol mixing, and, regardless of the magnitudes of either AOD or visibility, the column measurement of AOD is not a good representation of the surface measurement of b_{ext}, and
4) ASOS one-minute b_{ext} measurements truncate at 0.05 km^{-1}, which reduces the number of valid collocation points. This happens most often in winter.

5.2. Incorporation of GEOS-5 modeled aerosol vertical profile

As suggested above, one of the greatest challenges in using remote sensing technique to map geophysical parameters near the surface is the treatment of the shape of the vertical profile for that quantity. While most aerosol mass resides in the boundary layer near the surface, there are cases where aerosol is transported at elevation. Thus, knowing the vertical profile *a priori* can help to specify the column/surface relationship. Many past studies have incorporated vertical profile information from various sources such as LIDAR (e.g., Engel-Cox et al., 2006; Schaap et al., 2009) and global models (e.g., Liu et al., 2004; Van Donkelaar et al., 2006, 2010) to relate the AOD to surface PM2.5. A similar strategy is applied here.

Three methods of modeling visibility from MODIS AOD are developed in this study. The baseline method of applying regression equations between MODIS AOD and ASOS b_{ext} without any treatment of aerosol vertical profile will be called Method 0 (M0).

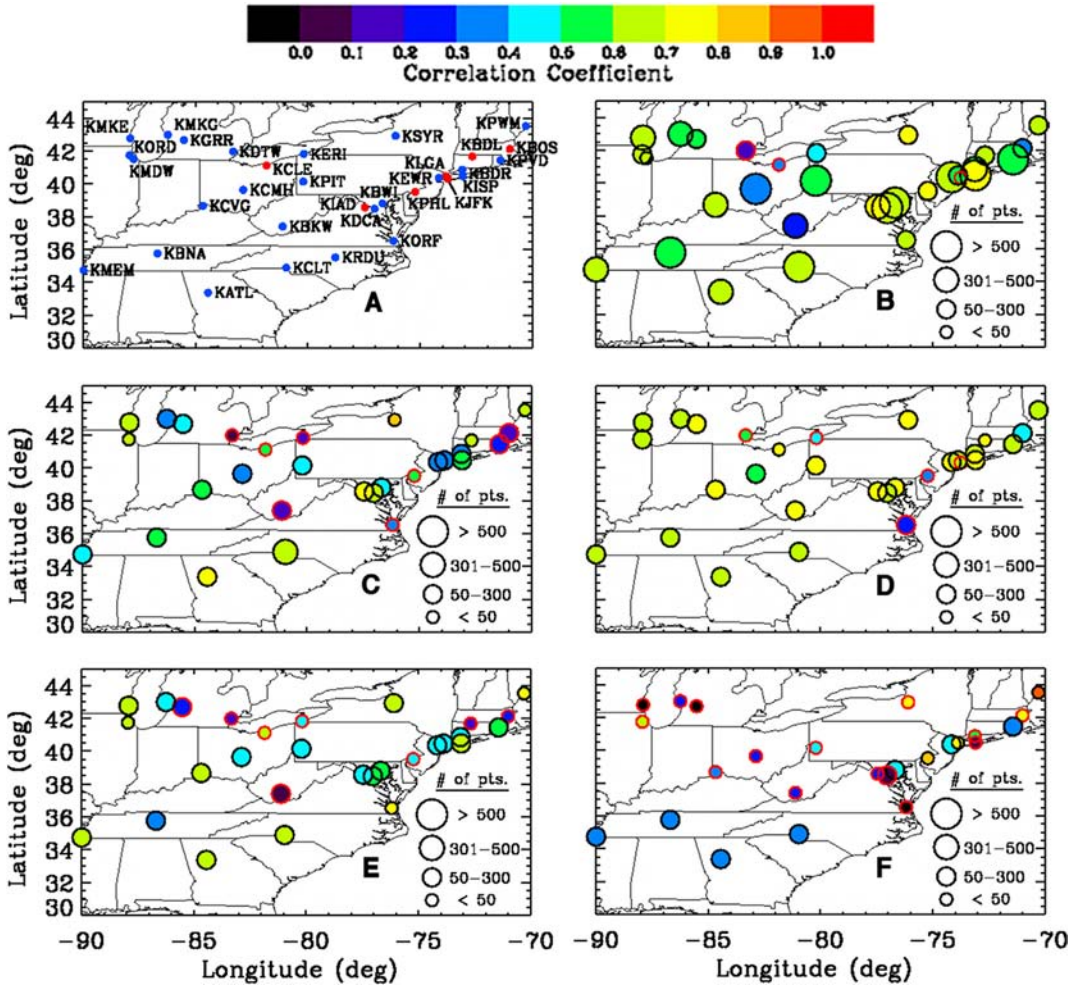

Fig. 3. (A) Map of ASOS stations used in long-term analysis. Blue circle stations have two visibility sensors. Red circle stations have three visibility sensors. (B) Map of the correlation between ASOS b_{ext} and MODIS AOD for the stations shown in (A) for the years 2000–2011. (C) Similar to (B) but for spring (MAM). (D) Similar to (B) but for summer (JJA). (E) Similar to (B) but for fall (SON). (F) Similar to (B) but for winter (DJF). In (B–F) circles outlined in red are not significant data.

The other two methods, as detailed below, incorporate simulated data from the NASA GEOS-5 MERRA Aerosol Reanalysis, such as planetary boundary layer height (PBLH) and surface extinction. For each method, three years of summer data (JJA) are analyzed (2003–2004, 2006) and then one summer of data is used as a 'test' summer (2005). Commonly used in the atmospheric sciences (Wilks, 2011), this leave-one-out cross validation strategy ensures that the robustness of the statistical prediction model can be evaluated independently (with the datasets not used in building the model). Only summer data are used in this next section as the long-term analysis results show that the best correlations between AOD and surface visibility occur during the summer months, and thus summer is the most favorable season to evaluate different methods.

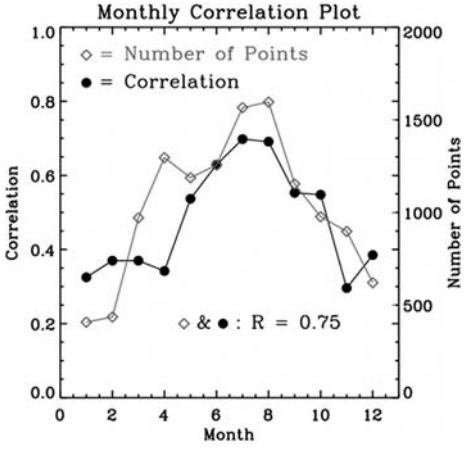

Fig. 4. Monthly correlation plot of ASOS b_{ext} versus MODIS AOD for the years 2000–2011 shown by black circles. Number of points used in monthly correlation calculation shown by gray diamonds.

5.2.1. Method 1

The first method (M1) that incorporates simulated data is based on Liu et al. (2004) and Wang et al. (2010). In this method, the GEOS-5 model is used to develop a scalar to multiply the MODIS AOD in order to derive b_{ext}. First, the mixing ratio of five species of aerosol (dust, sea salt, sulfate, black carbon, and organic carbon) is taken from GEOS-5 and then multiplied by the pressure thickness and the mass extinction efficiency of the aerosol in order to determine a simulated surface b_{ext} value. In the GEOS-5 model, aerosols are assumed to be mixed externally, and the RH-dependent mass extinction efficiency of different aerosol species are based upon the work by Hess et al. (1998) for sulfate and sea salt, by Chin et al. (2002) for black and organic carbon aerosols, and by Shettle and Fenn (1979) for dust particles; details and recent updates are summarized in Colarco et al. (2010). All sulfates are

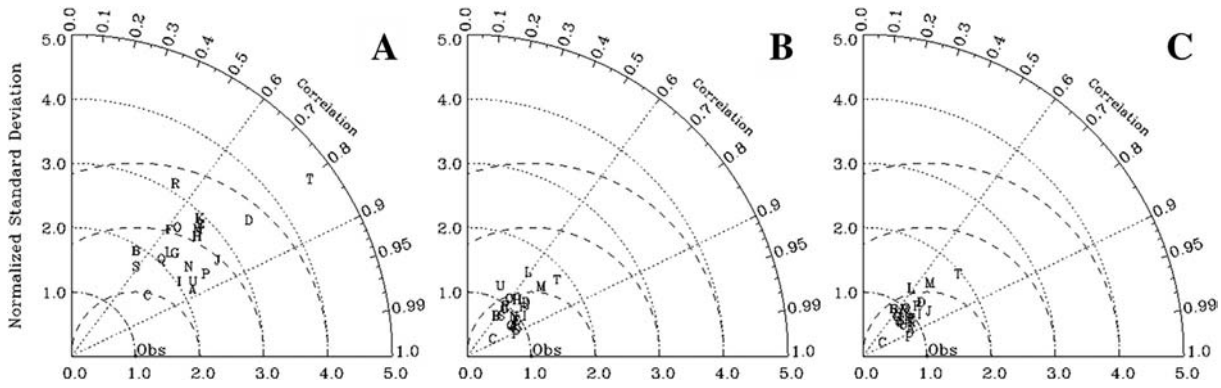

Fig. 5. Taylor Diagram showing correlation, normalized standard deviation, and normalized RMSD for 22 ASOS stations using (A) M0, (B) M1, and (C) M2. Key is located in Table 1.

assumed as ammonium sulfate, and no nitrate cycle is considered in GEOS-5.

In order to account for Rayleigh scattering in the atmosphere and its impairment on visibility, our method uses the parameterization scheme by Bodhaine et al. (1999). In the parameterization scheme, this study computes the concentration of CO_2 by averaging the June, July, and August monthly average CO_2 concentration for the years 2003–2006 as recorded at Mauna Loa, Hawaii (Keeling et al., 2009). Consequently, the following equation is used to determine a simulated extinction coefficient value for M1:

$$b_{\text{ext}} = \frac{b_{\text{ext\_G5}}(0)}{\text{AOD}_{\text{G5}}} \cdot \text{AOD}_{\text{M}} + b_{\text{Ray}} \tag{7}$$

where $b_{\text{ext\_G5}}(0)$ is the GEOS-5 modeled extinction at the lowest level of the model, AOD_{G5} is the modeled AOD, AOD_{M} is the retrieved AOD from MODIS, and b_{ray} is the calculated Rayleigh scattering.

5.2.2. Method 2

The second method (M2) is a combination of M1 and the 'well-mixed' method used in many PM-AOD studies (e.g. Tsai et al., 2011). In the 'well-mixed' method, the AOD within the PBL is assumed to be representative of the extinction at the surface. One problem with the 'well-mixed' method is that often aerosols are found to be above the PBL. To compensate for this problem, in M2 we scale the MODIS AOD with the ratio between GEOS-5 AOD below PBLH ($\text{AOD}_{\text{G5\_below}}$) and in the whole column in order to constrain AOD within the PBL, and thus the final equation is:

$$b_{\text{ext}} = \frac{\frac{\text{AOD}_{\text{G5\_below}}}{\text{AOD}_{\text{G5}}} \cdot \text{AOD}_{\text{M}}}{\text{PBLH}} + b_{\text{Ray}}. \tag{8}$$

5.3. Model development, results, and evaluations

To compare and evaluate M0, M1, and M2, we plot their results respectively in three Taylor Diagrams (Taylor, 2001; Fig. 5). In each diagram, the cosine of the polar angle represents the correlation, the radius of the circles centered at "Obs" represents the normalized root-mean-square-difference (RMSD), and the radius of the polar plot represents the normalized standard deviation (with respect to the counterpart of observation). The closer to the "Obs" point, the better the modeled result. Statistics in Fig. 5 are from the results for 22 ASOS stations for the summers of 2003, 2004, and 2006. Stations with $p > 0.01$ and fewer than four collocated points are not shown or included in the analysis (10 stations total).

Results are generally good for M0 with a mean correlation coefficient (R) of 0.74 and a median correlation of 0.73. However, M1 and M2 are closer to "Obs" than M0. M1 and M2 improve the mean correlation by 0.02 and 0.04, respectively, when compared to M0. They also improve the median correlation by 0.05 and 0.05, respectively. However, it is important to note neither of the methods universally improved the correlation for all stations when compared to M0. M1 improved the correlation for 55% of the stations while M2 improved the correlation for 64% of the stations.

The regression equations from Fig. 6A–C, respectively, are used to create three models to be tested in the summer of 2005. The first model (Mod0) is based on the results of M0:

$$b_{\text{ext}} = 0.46 \cdot \text{AOD}_{\text{M}} + 0.01. \tag{9}$$

The second model (Mod1) is based on the results of M1:

$$b_{\text{ext}} = 0.99 \cdot \frac{b_{\text{ext\_G5}}(0)}{\text{AOD}_{\text{G5}}} \cdot \text{AOD}_{\text{M}} + 0.03. \tag{10}$$

The third model (Mod2) is based on the results of M2:

$$b_{\text{ext}} = 1.03 \cdot \frac{\frac{\text{AOD}_{\text{G5\_below}}}{\text{AOD}_{\text{G5}}} \cdot \text{AOD}_{\text{M}}}{\text{PBLH}} + 0.04. \tag{11}$$

Independent validation results for the year 2005 are shown in Fig. 6D and E. Visibility is calculated for each model using Eq. (4). Mod0 results in a correlation of 0.57 with a linear regression of $\text{Vis}_{\text{Mod0}} = 1.91\ \text{Vis}_{\text{ASOS}} - 14.06$ (Fig. 6D). Mod1 shows an improvement in both correlation and regression over M0 with a correlation of 0.71 and a linear regression of $\text{Vis}_{\text{Mod1}} = 1.14\ \text{Vis}_{\text{ASOS}} - 0.49$ (Fig. 6E). The mean bias for Mod1 is ~3.6 km (Fig. 6E). Mod2 shows an improvement in both correlation and regression over Mod0 with $R = 0.70$, a linear regression of $\text{Vis}_{\text{Mod2}} = 0.98\ \text{Vis}_{\text{ASOS}} + 0.63$, and a mean bias of 0.32 km (Fig. 6F). Overall, Mod2 appears to be the best method as the difference in correlation amongst the models is negligible, and Mod2 shows the best regression, RMSE, and mean bias (Fig. 6D–F). However, because of the non-linearity between AOD and b_{ext}, the better performance of Mod2 doesn't mean that modeled b_{ext} below PBL (M2) correlates better with the ASOS ground-based observations than b_{ext} (M1); indeed, they show very similar correlations with ASOS b_{ext}.

5.4. A case study

To demonstrate the application of the best model, a visibility map for 11–14 August 2005 was created using Mod2 (Fig. 7A–D, respectively). During this time, a high-AOD event occurred over the East Coast of the United States, and a high-pressure system moved from the Kentucky region to the Atlantic Ocean, transporting and suppressing removal of smoke and sulfate aerosols in this area. In the visibility map, ASOS stations (denoted as circles in the map)

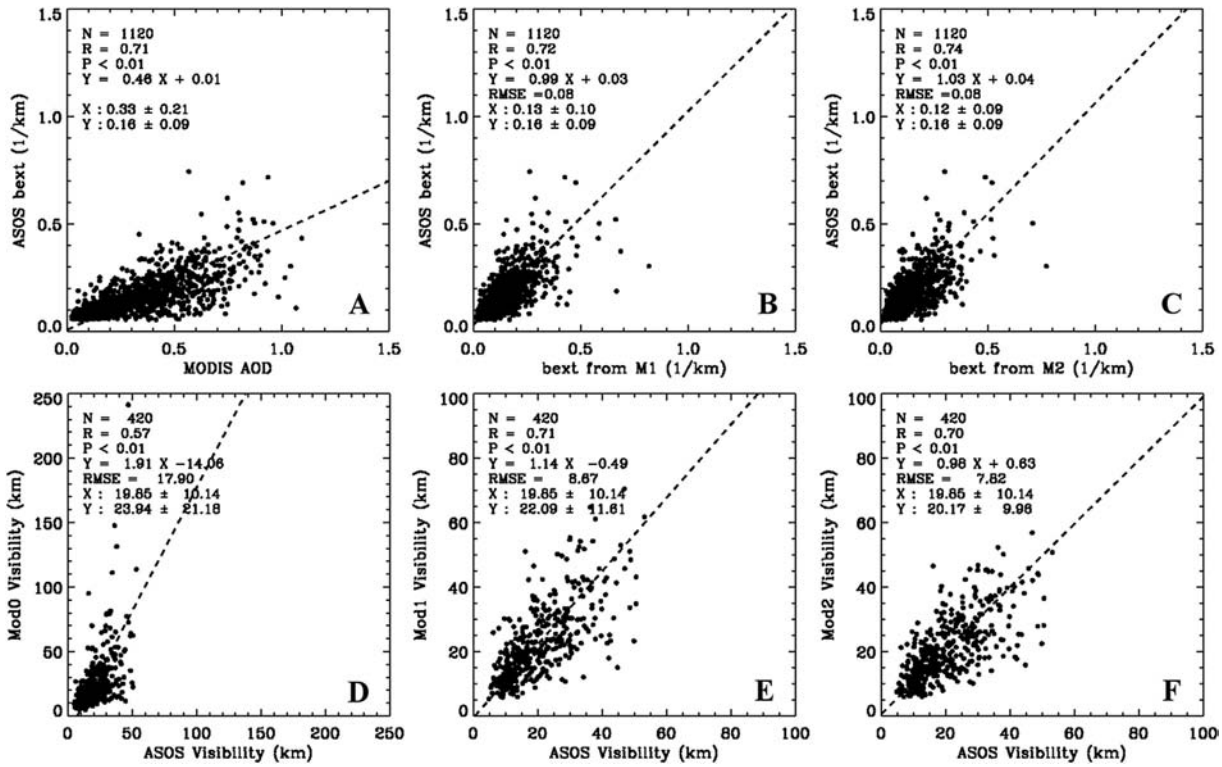

Fig. 6. Correlation plots of (A) MODIS AOD versus ASOS b_{ext} for 2003–2004 and 2006 (M0), (B) b_{ext} from M1 versus ASOS b_{ext} for 2003–2004 and 2006, (C) b_{ext} from M2 versus ASOS b_{ext} for 2003–2004 and 2006, (D) ASOS visibility versus Mod0 visibility for 2005, (E) ASOS visibility versus Mod1 visibility for 2005, and (F) ASOS visibility versus Mod2 visibility for 2005. Note that in (A)–(C) the ASOS data are on the *y*-axis as the method data (M0, M1, and M2) are an input parameter for predicting the ASOS data. However, in (D)–(F) ASOS data are used for validation purposes and hence the ASOS data are on the *x*-axis. Note also the difference in scales.

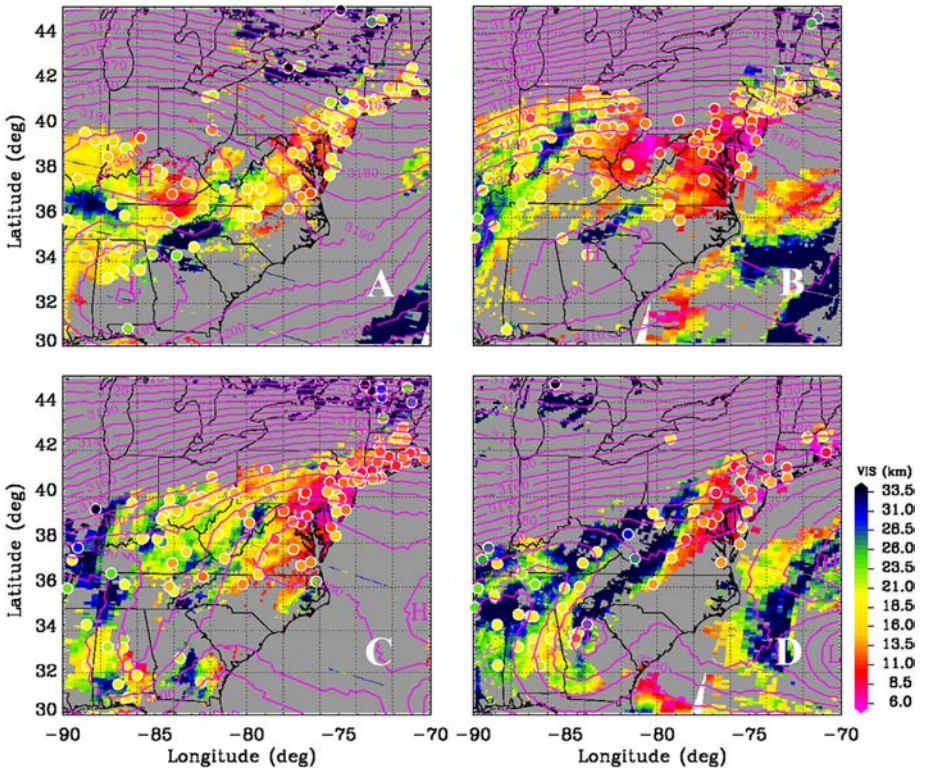

Fig. 7. Map of modeled visibility from Mod2 for (A–D, respectively) 11–14 August 2005. ASOS visibility is denoted by circles. Pink lines represent the North American Regional Reanalysis (NARR) 700-hPa geopotential heights. Gray coloring represents cloud.

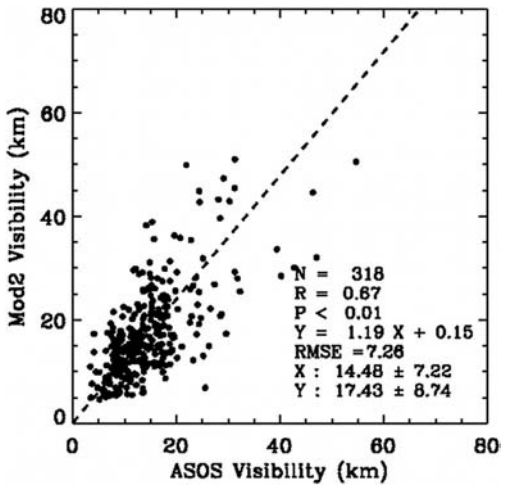

Fig. 8. Correlation plot of ASOS visibility versus Mod2 visibility for 11–14 August 2005.

containing one, two, and three sensors are included in order to ensure the maximum number of collocated data points for the purpose of demonstrating the possible applications of our method. Fig. 7 shows that in cases like this where the visibility has high spatial and temporal variability, ASOS stations (even after inclusion of single-sensor stations) may not be sufficient to capture the poor visibility events such as over highways where visibility information is highly needed. The satellite-derived visibility map, however, shows a much fuller picture of visibility at the surface. For instance, the 'hotspot' over southeast Kentucky and northeast Tennessee on 11 August (Fig. 7A), as seen by the satellite, has very little ASOS coverage. This clearly suggests that satellite-derived visibility can be used as a supplement to meet the operational needs of visibility information.

The correlation between ASOS visibility and Mod2 visibility for all four days of data is 0.67 (Fig. 8). The root mean square error (RMSE) is 7.26 and the mean bias is 2.95 km, signifying that Mod2 tends to slightly overestimate visibility. Nevertheless, it appears that the model we established in the analysis of 3-years of summer data is representative for the summer in our study region, and can be applied operationally for future years, but could be improved upon in future studies.

6. Summary and conclusions

Surface visibility has important implications for air quality, transportation and safety, but current measurements of visibility lack spatial coverage. This study aims to discover the feasibility of using satellite retrievals of AOD to determine surface visibility. First, a quality control regime was developed for the ASOS one-minute extinction coefficient (b_{ext}) data. This regime includes four criteria that must be met by each data point, resulting in an average data loss of 66.9% for all 32 stations used in this study. This large quantity of data loss is justified by the assurance that only data of the highest quality are retained and analyzed.

A long-term analysis of 32 East Coast ASOS stations for the years 2000–2011 was performed, and an average correlation between MODIS AOD and ASOS b_{ext} of 0.61 was found for all stations. This analysis shows that the relationship between MODIS AOD and ASOS b_{ext} is greatest during the summer months and lowest during the winter months. The highest monthly correlation of 0.70 is found in July, while the lowest correlation of 0.30 is found in November. The good correlation during the summer months is likely due to a well-mixed PBL during the summer, and thus the column measurement of b_{ext} is a good representation of the surface measurement of b_{ext}. Furthermore, a strong relationship ($R = 0.75$) was found between the monthly correlation value and the number of points used in the analysis. Thus, the higher correlation values during the summer might also be partially attributable to a greater number of collocated points.

Data from the NASA GEOS-5 MERRA Aerosol Reanalysis were used to determine the vertical profile of aerosol in order to develop two methods for deriving visibility from MODIS AOD. These methods were compared with a baseline method that uses regression between MODIS AOD to ASOS b_{ext} (M0). The first method (M1) scales the modeled surface extinction coefficient with the ratio between MODIS AOD and the modeled AOD. The second method (M2) scales the modeled AOD within the PBL with the ration between MODIS AOD and modeled AOD and then divides it by the height of the PBL. These methods, along with (M0), were used to develop three models to be tested for the summer of 2005 (Mod0, Mod1, and Mod2). Mod2 showed the best results with a means bias of 0.32 km, an RMSE of 7.82, and a correlation of 0.70.

To demonstrate the feasibility of our method, Mod2 was applied to a high-AOD case study during the time period of 11–14 August, 2005. Mod2 visibility was compared with ASOS visibility. Results were generally good with a correlation of 0.67 for all four days and a mean bias of ~3 km.

Currently, there is a lack of spatial coverage of surface visibility measurements. Satellites have the capability of global spatial coverage. This study shows a good relationship between remotely sensed AOD and surface visibility at airports across the East Coast of the United States. This relationship can generally be improved with the incorporation of modeled aerosol vertical profile information, promoting the possibility of global surface visibility measurements from remotely sensed AOD. However, this study focused on regions that are often located in or near cities, and thus have high levels of aerosol. Remote sensing of visibility will likely prove to be more difficult in regions and times (e.g. winter) where visibility is generally good because satellite remote sensing of aerosols is more challenging in low AOD conditions, especially over land. Interestingly, any visibility larger than 10 miles is truncated in the operational weather observation report. Hence, this study at least shows the potential of using satellite AOD to derive the surface visibility that can be comparable with operationally reported visibility from ground observations. But, further studies are needed to evaluate the method of this study with visibility data from regions that have low AOD such as the Interagency Monitoring of Protected Visual Environments (IMPROVE) sites that are located at national parks and wilderness areas. Another challenge to the derivation of surface visibility from remotely sensed AOD is the incorporation of the vertical profile of aerosol. Two possible methods were shown in this study. These methods may be improved in future studies through an integrated combination of satellite radiances, aerosol vertical profiles from lidar, and chemistry transport models.

Acknowledgments

This work was partially funded by the NASA Nebraska Space Grant student fellowship and mini-grant program as well as the NASA GSFC Graduate Student Summer Program and Senior Internship Program (Kessner). This research is also partially supported by the NASA Applied Sciences Program managed by Lawrence A. Friedl and John A. Haynes. We thank the data services provided by the Goddard Earth Sciences Data Center and the National Climatic Data Center Online Climate Data Directory. We

would like to give a special thanks to the employees of Belfort Instrument, Lorraine A. Remer, Raymond M. Hoff, and R. Bradley Pierce for their guidance and expertise.

References

Allen, G., Sloutas, C., Koutrakis, P., Reiss, R., Lurmann, F.W., Roberts, P.T., 1997. Evaluation of the TEOM method for measurement of ambient particulate mass in urban areas. J. Air Waste Manag. Assoc. 47 (6), 682–689.

Bodhaine, B.A., Wood, N.B., Dutton, E.G., Slusser, J.R., 1999. On Rayleigh optical depth calculations. J. Atmos. Ocean. Technol. 16 (11), 1854–1861.

Chin, M., Ginoux, P., Kinne, S., Torres, O., Holben, B., Duncan, B., Martin, R., Logan, J., Higurashi, A., Nakajima, T., 2002. Tropospheric aerosol optical thickness from the GOCART model and comparisons with satellite and sun photometer measurements. J. Atmos. Sci. 59 (3), 461–483.

Cismoski, D.S., 1994. Nephelometer Data Reduction and Validation (IMPROVE PROTOCOL). Air Resource Specialists, Inc, Fort Collins, Colorado.

Colarco, P., da Silva, A., Chin, M., Diehl, T., 2010. Online simulations of global aerosol distributions in the NASA GEOS-4 model and comparisons to satellite and ground-based aerosol optical depth. J. Geophys. Res. 115 (D14), D14207. http://dx.doi.org/10.1029/2009JD012820.

Crosby, J.D., 2003. Visibility Sensor Accuracy: What's Realistic? EnviroTech Sensors, Inc, Clarksville, Maryland.

Dee, D.P., Da Silva, A.M., 1998. Data assimilation in the presence of forecast bias. Quart. J. R. Meteorol. Soc. 124 (545), 269–295.

Dee, D.P., Da Silva, A.M., 1999. Maximum-likelihood estimation of forecast and observation error covariance parameters. Part I: methodology. Mon. Weather Rev. 127 (8), 1822–1834.

Dee, D.P., Rukhovets, L., Todling, R., Da Silva, A.M., Larson, J.W., 2001. An adaptive buddy check for observational quality control. Quart. J. R. Meteorol. Soc. 127 (577), 2451–2471.

EG&G Electro-Optics, 1983. High Efficiency Bulb Type Xenon Flashtubes and Litepac Trigger Modules (Salem, Massachusetts).

Engel-Cox, J.A., Hoff, R.M., Rogers, R., Dimmick, F., Rush, A.C., Szykman, J.J., Al-Saadi, J., Chu, D.A., Zell, E.R., 2006. Integrating lidar and satellite optical depth with ambient monitoring for 3-dimensional particulate characterization. Atmos. Environ. 40 (40), 8056–8067.

Fei, H., Hong, W., Junping, Q., Guofu, W., 2006. Retrieval of atmospheric horizontal visibility by statistical regression from NOAA/AVHRR satellite data. J. Ocean Univ. China 5 (3), 207–212. http://dx.doi.org/10.1007/s11802-006-0003-4.

Green, M., Kondragunta, S., Ciren, P., Xu, C., 2009. Comparison of GOES and MODIS Aerosol Optical Depth (AOD) to Aerosol Robotic Network (AERONET) AOD and improve PM2.5 mass at Bondville, Illinois. J. Air Waste Manag. Assoc. 59 (9), 1082–1091. http://dx.doi.org/10.3155/1047-3289.59.9.1082.

Gupta, P., Christopher, S.A., Wang, J., Gehrig, R., Lee, Y., Kumar, N., 2006. Satellite remote sensing of particulate matter and air quality assessment over global cities. Atmos. Environ. 40 (30), 5880–5892. http://dx.doi.org/10.1016/j.atmosenv.2006.03.016.

Hadjimitsis, D.G., Clayton, C., Toulios, L., 2010. Retrieving visibility values using satellite remote sensing data. Phys. Chem. Earth 35 (1), 121–124.

Hess, M., Koepke, P., Schult, I., 1998. Optical properties of aerosols and clouds: the software package OPAC. Bull. Am. Meteorol. Soc. 79 (5), 831–844.

Hoff, R.M., Christopher, S.A., 2009. Remote sensing of particulate pollution from space: have we reached the promised land? J. Air Waste Manag. Assoc. 59 (6), 645–675 http://dx.doi.org/10.3155/1047-3289.59.6.645.

Ichoku, C., Chu, D.A., Mattoo, S., Kaufman, Y.J., Remer, L.A., Tanré, D., Slutsker, I., Holben, B.N., 2002. A spatio-temporal approach for global validation and analysis of MODIS aerosol products. Geophys. Res. Lett. 29 (12), 8006. http://dx.doi.org/10.1029/2001GL013206.

Kaufman, Y.J., Fraser, R.S., 1983. Light extinction by aerosols during summer air pollution. J. Clim. Appl. Meteorol. 22, 1694–1706.

Keeling, R.F., Piper, S.C., Bollenbacher, A.F., Walker, J.S., 2009. Atmospheric CO_2 records from sites in the SIO air sampling network. In: Trends: a Compendium of Data on Global Change. Carbon Dioxide Information Analysis Center, Oak Ridge National Laboratory, U.S. Department of Energy, Oak Ridge, Tenn., U.S.A. http://dx.doi.org/10.3334/CDIAC/atg.035.

Koelemeijer, R.B.A., Homan, C.D., Matthijsen, J., 2006. Comparison of spatial and temporal variations of aerosol optical thickness and particulate matter over Europe. Atmos. Environ. 40, 5304–5315. http://dx.doi.org/10.1016/j.atmosenv.2006.04.044.

Levy, R.C., Remer, L.A., Tanré, D., Kaufman, Y.J., Ichoku, C., Holben, B.N., Livingston, J.M., Russell, P.B., Maring, H., 2003. Evaluation of the Moderate-Resolution Imaging Spectroradiometer (MODIS) retrievals of dust aerosol over the ocean during PRIDE. J. Geophys. Res. 108 (D19), 8594. http://dx.doi.org/10.1029/2002JD002460.

Levy, R.C., Remer, L.A., Mattoo, S., Vermote, E.F., Kaufman, Y.J., 2007. Second-generation operational algorithm: retrieval of aerosol properties over land from inversion of moderate resolution imaging spectroradiometer spectral reflectance. J. Geophys. Res. 112, D13211. http://dx.doi.org/10.1029/2006JD007811.

Liu, Y., Park, R.J., Jacob, D.J., Li, Q., Kilaru, V., Sarnat, J.A., 2004. Mapping annual mean ground-level $PM_{2.5}$ concentrations using multiangle imaging spectroradiometer aerosol optical thickness over the contiguous United States. J. Geophys. Res. 109, D22206. http://dx.doi.org/10.1029/2004JD005025.

Mensah, E.K., Osei-Adjei, S., 1991. Traffic accidents time value and the benefits of improvements in environmental visibility. J. Environ. Sys. 21 (1), 53–63.

Molenar, J.V., Cismoski, D.S., Tree, R.M., 1992. Intercomparison of Ambient Optical Monitoring Techniques. Air Resource Specialists, Inc, Fort Collins, Colorado.

National Climatic Data Center, 2003. Data Documentation for Data Set 3285 (DSI-3285): ASOS Surface 1 Minute Data (Asheville, North Carolina).

National Oceanic and Atmospheric Administration, Department of Defense, Federal Aviation Administration, and United States Navy, 1998. Automated Surface Observing System (ASOS) User's Guide.

Qu, W., Wang, J., Gao, S., Wu, T., 2013. Effect of the strengthened western Pacific subtropical high on summer visibility decrease over eastern China. J. Geophys. Res. Atmos. 118, 7142–7156. http://dx.doi.org/10.1002/jgrd.50535.

Remer, L.A., Tanré, D., Kaufman, Y.J., Levy, R., Mattoo, S., 2009. Algorithm for Remote Sensing of Tropospheric Aerosol from MODIS for Collection 005: Revision 2. Goddard Space Flight Center/National Aeronautics and Space Administration, Greenbelt, MD.

Retalis, A., Hadjimitsis, D.G., Michaelides, S., Tymvios, F., Chrysoulakis, N., Clayton, C.R.I., Themistocleous, K., 2010. Comparison of aerosol optical thickness with in situ visibility data over Cyprus. Nat. Haz. Earth Sys. Sci. 10, 421–428.

Richards, L.W., Dye, T.S., Arthur, M., Byars, M.S., 1996. Analysis of ASOS Data for Visibility Purposes. Final Report. Systems Applications International, Inc, San Rafael, California.

Rienecker, M.M., Suarez, M.J., Todling, R., Bacmeister, J., Takacs, L., Liu, H.–C., Gu, W., et al., 2008. The GEOS-5 Data Assimilation System–Documentation of Version 5.0.1, 5.1.0, and 5.2.0. NASA Technical Report Series on Global Modeling and Data Assimilation 27 (December 30), pp. 1–118.

Rienecker, M.M., et al., 2011. MERRA: NASA's modern-era for research and applications. J. Clim. 24 (14), 3624–3648. http://dx.doi.org/10.1175/JCLI-D-11-00015.1.

Schaap, M., Apituley, A., Timmermans, R.M.A., Koelemeijer, R.B.A., De Leeuw, G., 2009. Exploring the relation between aerosol optical depth and $PM_{2.5}$ at Cabauw, the Netherlands. Atmos. Chem. Phys. 9, 909–925.

Shettle, E., Fenn, R.W., 1979. Models for the Aerosols of the Lower Atmosphere and the Effects of Humidity Variations on Their Optical Properties. AFGL-TR-79-0214. U.S. Air Force Geophysics Laboratory, Hanscom Air Force Base, Mass, pp. 1–94.

Takemura, T., Nakajima, T., Dubovik, O., Holben, B.N., Kinne, S., 2002. Single-scattering albedo and radiative forcing of various aerosol species with a global three-dimensional model. J. Clim. 15 (4), 333–352.

Tang, I.N., Munkelwitz, H.R., 1994. Water activities, densities, and refractive indices of aqueous sulfates and sodium nitrate droplets of atmosphere importance. J. Geophys. Res. 99 (D9), 18801–18808.

Taylor, K.E., 2001. Summarizing multiple aspects of model performance in a single diagram. J. Geophys. Res. 106 (D7), 7183–7192.

Trijonis, J., Thayer, M., Murdoch, J., Hageman, R., 1985. Air Quality Benefit Analysis for Los Angeles and San Francisco Based on Housing Values and Visibility. Final Report to the California Air Resources Board. Sacramento, California, Contract A2-088-32.

Tsai, T.-C., Jeng, Y.-J., Chu, D.A., Chen, J.-P., Chang, S.-C., 2011. Analysis of the relationship between MODIS aerosol optical depth and particulate matter from 2006 to 2008. Atmos. Environ. 45 (27), 4777–4788. http://dx.doi.org/10.1016/j.atmosenv.2009.10.006.

U.S. Environmental Protection Agency (USEPA), Office of Air and Radiation, 2011. The Benefits and Costs of the Clean Air Act from 1990 to 2020. Final Report – Rev. A http://www.epa.gov/oar/sect812/prospective2.html.

Van Donkelaar, A., Martin, R.V., Park, R.J., 2006. Estimating ground-level $PM_{2.5}$ using aerosol optical depth determined from satellite remote sensing. J. Geophys. Res. 111, D21201. http://dx.doi.org/10.1029/2005JD006996.

Van Donkelaar, A., Martin, R.V., Brauer, M., Kahn, R., Levy, R., Verduzco, C., Villeneuve, P.J., 2010. Global estimates of ambient fine particulate matter concentrations from satellite-based aerosol optical depth: development and application. Environ. Health Perspect. 118 (6), 847–855.

Vermote, E.F., Vibert, S., Kilcoyne, H., Hoyt, D., Zhao, T., 2002. Suspended Matter: Visible/Infrared Imager/Radiometer Suite Algorithm Theoretical Basis Document. Raytheon Systems Company, Information Technology and Scientific Services, Maryland.

Wang, J., Christopher, S.A., 2003. Intercomparison between satellite-derived aerosol optical thickness and $PM_{2.5}$ mass: implications for air quality studies. Geophys. Res. Lett. 30 (21), 2095. http://dx.doi.org/10.1029/2003GL018174.

Wang, J., Hoffmann, A.A., Park, R., Jacob, D.J., Martin, S.T., 2008. Global distribution of solid and aqueous sulfate aerosols: effect of the hysteresis of particle phase transitions. J. Geophys. Res. 113, D11206.

Wang, J., Nair, U., Christopher, S.A., 2004. GOES-8 Aerosol optical thickness assimilation in a mesoscale model: Online integration of aerosol radiative effects. J. Geophys. Res. 109, D23203. http://dx.doi.org/10.1029/2004JD004827.

Wang, J., Xu, X., Spurr, R., Wang, Y., Drury, E., 2010. Improved algorithm for MODIS satellite retrievals of aerosol optical thickness over land in dusty atmosphere: implications for air quality monitoring in China. Remote Sens. Environ. 114, 2575–2583.

Watson, J.G., Chow, J.C., 1994. Clear sky visibility as a challenge for society. Annual Review of Energy and the Environment 19 (1), 241–266. http://dx.doi.org/10.1146/annurev.eg.19.110194.001325.

Watson, J.G., Fujita, E., Chow, J.C., Zielinska, B., 1998. Northern Front Range Air Quality Study Final Report Colorado State University. Office of the Vice President for Research and Information Technology.

Wang, K., Dickinson, R.E., Liang, S., 2009. Clear sky visibility has decreased over land globally from 1973 to 2007. Science 323, 1468–1470. http://dx.doi.org/10.1126/science.1167549.
Wilks, D.S., 2011. Statistical forecasting. In: Statistical Methods in the Atmospheric Sciences, third ed. Elsevier, Oxford, pp. 252–254.
World Meteorological Organization, 2008. Guide to Meteorological Instruments and Methods of Observation, seventh ed. WMO-No. 8, Geneva, Switzerland.
Xu, X., Wang, J., Henze, D.K., Qu, W., Kopacz, M., 2013. Constraints on aerosol sources using GEOS-Chem adjoint and MODIS radiances, and evaluation with multisensor (OMI, MISR) data. J. Geophys. Res. Atmos. 118. http://dx.doi.org/10.1002/jgrd.50515.
Zhang, H., Hoff, R.M., Engel-Cox, J.A., 2009. The relation between Moderate Resolution Imaging Spectroradiometer (MODIS) aerosol optical depth and PM2.5 over the United States: a geographical comparison by U.S. Environmental Protection Agency regions. J. Air Waste Manag. Assoc. 59 (11), 1358–1369.